Bulushev, D. A., Zacharska, M., Lisitsyn, A. S., Podyacheva, O. Y., Hage, F. S., Ramasse, Q. M., Bangert, U., and Bulusheva, L. G. (2016) Single atoms of Pt-group metals stabilized by N-doped carbon nanofibers for efficient hydrogen production from formic acid. ACS Catalysis, 6(6), pp. 3442-3451.

There may be differences between this version and the published version. You are advised to consult the publisher's version if you wish to cite from it.

http://eprints.gla.ac.uk/131172/

Deposited on: 9 November 2016

Enlighten – Research publications by members of the University of Glasgow
http://eprints.gla.ac.uk

Single Atoms of Pt-Group Metals Stabilized by N-Doped Carbon Nanofibers for Efficient Hydrogen Production from Formic Acid

Dmitri A. Bulushev,*[†,‡,#] Monika Zacharska,[§,⊥] Alexander S. Lisitsyn,[†] Olga Yu. Podyacheva,[†,‡] Fredrik S. Hage,[∥] Quentin M. Ramasse,[∥] Ursel Bangert,[⊥] and Lyubov G. Bulusheva[#,‡]

Published in ACS Catalysis, 2016, v. 6, p. 3442-3451.

[†]Boreskov Institute of Catalysis, SB RAS, 630090 Novosibirsk, Russia

[‡]Novosibirsk State University, 630090 Novosibirsk, Russia

[§]Chemical & Environmental Sciences Department, University of Limerick, Limerick, Ireland

[⊥]Materials & Surface Science Institute, University of Limerick, Limerick, Ireland

[∥]SuperSTEM, STFC Daresbury Laboratories, Warrington, United Kingdom

[#]Nikolaev Institute of Inorganic Chemistry, SB RAS, 630090 Novosibirsk, Russia

* E-mail: dmitri.bulushev@catalysis.ru

ABSTRACT

Formic acid is a valuable chemical derived from biomass, as it has a high hydrogen-storage capacity and appears to be an attractive source of hydrogen for various applications. Hydrogen production via formic acid decomposition is often based on using supported catalysts with Pt-group metal nanoparticles. In the present paper, we show that the decomposition of the acid proceeds more rapidly on single metal atoms (by up to one order of magnitude). These atoms can be obtained by rather simple means through anchoring Pt-group metals onto mesoporous N-functionalized carbon nanofibers. A thorough evaluation of the structure of the active site by aberration-corrected scanning transmission electron microscopy (ac-STEM) in high-angle annular dark field (HAADF) mode, by CO chemisorption, X-ray photoelectron spectroscopy (XPS) and quantum-chemical calculations reveals that the metal atom is coordinated by a pair of pyridinic nitrogen atoms at the edge of graphene sheets. The chelate binding provides an ionic/electron-deficient state of these atoms prevents their aggregation and thereby leads to an excellent stability under the reaction conditions. Catalysts with single atoms have also shown very high selectivity. Evidently, the findings can be extended to hydrogen production from other chemicals and can be helpful for improving other energy-related and environmentally benign catalytic processes.

Keywords: nitrogen-doped carbon; single-atom catalysts; hydrogen production; formic acid; renewable biomass

1. INTRODUCTION

Formic acid represents one of the most attractive hydrogen sources, as the content of hydrogen is relatively high (4.4 wt.%) and the hydrogen readily evolves upon catalytic decomposition at low temperatures.[1-5] It is also important that the starting acid can be produced with high yields from renewable biomass by hydrolysis of cellulose[6] or by its oxidation.[5,7] Additionally, formic acid can be used directly for hydrogenation reactions instead of molecular hydrogen, providing the advantage of easier transportation and storage of the hydrogenating agent.[8,9] Now, supported noble metal catalysts containing metal nanoparticles are mostly applied for the dehydrogenation of formic acid into H_2 and CO_2. However, the basic process is accompanied by undesired dehydration of formic acid into CO and H_2O, and this leads to a search for more efficient catalysts.

There is rather limited evidence of single-atom heterogeneous catalysis with noble metals. Catalysts dispersed into single atoms are considered as "atom-efficient",[10-12] since they allow the use of all atoms of the active component in the catalytic reaction, in contrast to catalysts with metallic nanoparticles, where a significant part of the expensive metal is located in the bulk of the nanoparticles and is inaccessible to the reactants. However, the advantage of the single active site is only realized if it possesses the same (or a higher) catalytic activity than the metal atoms on the surface of a nanoparticle. Unfortunately, this does not always happen, and single metal atoms can be less active and even inactive in some of the reactions.[13,14] The major applications of single-atom catalysis are currently related to environmental catalysis, e.g. to CO[15-17] or NO[18] oxidation, hydrogenation[16,19,20] and partial oxidation[21] reactions. Catalysis for energy applications is presented by electrocatalytic reactions[14,22] and by catalytic hydrogen-producing reactions such as reforming of naphtha,[23] formic acid decomposition,[24] and water-gas shift reaction.[12,25]

For the production of hydrogen by formic acid decomposition, catalysis with single-atoms and sub-nanometer clusters was reported for gold catalysts.[24,26,27] Evidently, the properties and

catalytic applications of single-atom catalysts should be strongly dependent on the catalyst's support. As a rule, metal oxides are used as supports for the catalysts. Carbon based supports have been used to a lesser extent so far,[14,16,19,22,28] probably, because of their weaker interaction with single metal atoms, which causes metal sintering and deactivation. Doping of the carbon support with foreign atoms may open a way for stabilizing the metal atoms. Nitrogen-containing carbon materials demonstrate a great potential for applications not only in catalysis, but also in different energy-related fields, such as fuel cells, batteries, supercapacitors, and hydrogen storage materials.[29,30] At the same time, intensive studies of these materials have started only recently. An important question is whether the N-functionalized carbon materials can stabilize single noble metal atoms as active sites for catalytic reactions. Interestingly, Arrigo et al.[14] reported that single Pd atoms supported on N-doped carbon nanotubes were inactive in phenylacetylene hydrogenation and CO oxidation, but active in the oxygen reduction reaction. It can be supposed that some hydrogen-producing reactions, such as formic acid[31,32] and ammonia[33] decomposition, which have been catalyzed by highly dispersed Pt-group metal catalysts supported on N-doped carbon materials, also take place on single metal atoms, though this needs confirmation.

Recently, we have reported that single Pd^{2+} atoms supported on N-doped graphene-like carbon could be the active sites for the formic acid decomposition reaction.[34] In the present paper, we show that the homogeneous precipitation of Pt, Pd or Ru onto another type of carbon – N-doped carbon nanofibers (N-CNFs) greatly improves the catalyst performance in the selective production of H_2 from formic acid, in comparison to the properties of the same metals on N-free CNFs. We perform an extended aberration-corrected HAADF/STEM studies to observe both metal nanoparticles and single metal atoms in the samples. To elucidate further the nature of the active sites in the catalysts, we compare CO chemisorption data, and X-ray photoelectron spectroscopy (XPS) results for the N-free and N-doped Pt-group samples. Moreover, we use density functional theory (DFT) calculations to reveal the location of metal species on N-doped carbon and to provide insights into the reasons of their specific catalytic properties. It was somewhat surprising to find that

the N-doped CNFs are able to behave as an efficient macro-ligand, which anchors firmly the individual metal atoms by the pyridinic nitrogen atoms located at the open graphene edges, thus preventing metal sintering and assuring catalyst stability at elevated temperatures, while the structure of the active site formed proves ideal for the formic acid decomposition to proceed with a high rate and exclusively to H_2 and CO_2.

2. METHODS

Materials. Carbon nanofibers (CNFs) and N-doped carbon nanofibers (N-CNFs) were synthesized by decomposition of ethylene and, accordingly, a mixture of ethylene and ammonia (1:3) on a 65 wt.% Ni/25 wt.% Cu/10 wt.% Al_2O_3 catalyst at 823 K for 1 h as was described earlier.[31,32,35] To remove the catalyst from the obtained materials, they were treated with concentrated HCl several times for several weeks at room temperature and then boiled in 2 M HCl for 30 min. After this, the materials were washed with distilled water until no chloride ions were detected in the rinsing liquid. Despite the severe treatment, some carbon supports contained encapsulated Ni carbide particles (Figure S1, Supporting Information) of about the diameter of the fibers in size in accordance with the literature data.[13,32,35] These Ni containing particles were distinctly different from the observed by HAADF/STEM Pt-group metal species in the catalysts, and in contrast to them, they were inactive in the formic acid decomposition reaction. The obtained supports CNFs and N-CNFs (7 wt.% N) were mesoporous with average pore diameters of 8 and 11 nm and Brunauer-Emmett-Teller (BET) surface areas of 220 and 200 $m^2\ g^{-1}$, respectively.

1 wt.% Ru and Pd catalysts on the N-free and N-doped carbon (1Ru/(N-)CNFs and 1Pd/(N-CNFs) were prepared via incipient wetness impregnation using an aqueous solution of $Ru(NO)(NO_3)_3$ or Pd-acetate in acetone, respectively. For the preparation of 0.3Pt/N-CNFs, 1Pt/CNFs and 1Pt/N-CNFs catalysts, 0.3 and 1 wt.% of Pt were deposited by homogeneous precipitation from H_2PtCl_6 with NaOH.[31] A known amount of acid was added to an aqueous

suspension of the support and stirred for 60 min at room temperature. Then, a stoichiometric amount of 0.5 M solution of NaOH was added drop-wise at room temperature. The mixture was stirred and heated for 1.5 h at 343 K. This was followed by filtration, careful washing of the material with distilled water, and drying. All the samples were finally reduced in flowing H_2 at 523-573 K for 1-2 hours. Unsupported Pt and Pd black powders with BET surface areas of 30 and 20 m^2 g^{-1}, respectively, were purchased from Alfa Aesar.

Instrumentation. Chemisorption measurements were performed on an AutoChem II 2920 (Micromeritics) in pulse mode,[36] using CO as the adsorbing gas and He as the carrier gas. The catalyst samples were reduced during preparation and were re-reduced before CO chemisorption under mild conditions. About 100 mg of sample were loaded into the quartz tube for the measurements, the tube was purged with He and the sample was then heated in flowing H_2 to 373 K and kept under H_2 for 10 min. Following cooling, purging of the sample tube with He, and stabilizing the temperature at 294±1 K, the sample was dosed with CO by 70 μL STP pulses, in 2-min intervals, until apparent saturation (constancy in the peak area) occurred.

A conventional JEOL JEM-2100F transmission electron microscope with an acceleration voltage of 200 kV was used to determine the morphology of the catalysts and the mean metal particle sizes. A probe corrected Nion UltraSTEM 100 scanning transmission electron microscope[37] was used at an acceleration voltage of 100 kV in bright field (BF) and high-angle annular dark-field (HAADF) imaging mode, the latter to reveal single metal atoms in the samples as the intensity in HAADF images is to a good approximation proportional to the atomic number (Z) as Z^n, $n \approx 1.7$.

X-ray photoelectron spectroscopy (XPS) measurements were performed on an AXIS Ultra DLD spectrometer (Kratos) using monochromatic Al Kα radiation (1486.6 eV). The C 1s line at 284.8 eV was taken as a reference for the energy calibration. Before the measurements, the samples were re-reduced *ex situ* in a preparation chamber of the XPS unit at 33 Pa of hydrogen at 573 K for 30 min and transferred to the measurement chamber in ultrahigh vacuum conditions (10^{-6} Pa) without contact with air.

Catalytic studies. Vapor-phase formic acid decomposition was carried out in a fixed bed 4 mm (i.d.) quartz reactor, as was described earlier.[32,38] Activity tests were performed at atmospheric pressure with catalyst loadings of 7 mg. All the catalysts were re-reduced in an 1 vol.% H_2/Ar mixture for 1 h at 573 K and cooled in He to the reaction temperature. To evaluate the temperature dependence of the acid conversion, the composition of the outlet gas mixture was measured several times at each temperature (at least for 30 min, to ensure that the activity was stable in time). The reaction mixture contained 1.8 vol.% of formic acid in He. All experiments were performed at a total flow rate of 51 mL^3 (STP) min^{-1}. The reactants and products were analyzed with a gas chromatograph (HP-5890) fitted with a Porapak-Q column and a thermal conductivity detector.

As there were no other carbon-containing products apart from CO and CO_2, the degree of conversion of formic acid was determined as the sum of their concentrations related to the initial concentration of formic acid. Turnover frequencies (TOFs) were calculated at low conversions (<20%) and were related to the total number of metal atoms in the sample. For the unsupported Pt and Pd powders, the TOFs were calculated based on the surface concentration of metal atoms, as found from the BET surface areas.

Computational details. Theoretical calculations were carried out using the gradient-corrected functional of Perdew-Burke-Ernzerhof (PBE) with local and nonlocal exchange and correlation[39] within the quantum-chemical program package Jaguar (Jaguar, version 7.9, Schrödinger, LLC, New York, NY, 2012). The hydrogen-terminated graphene fragments with graphitic- (N_{gr}) and pyridine-type (N_{py}) nitrogen atoms reflected the N-doped carbon substrate. The graphene fragments with a Pt-group metal atom located at an N site were calculated using a LACVP basis set, where the outermost core orbitals were included for metal and the 6-31G set was applied for light elements. For calculating the interaction of formic acid molecules with a catalyst, we used the LACVP*+ basis set with polarization functions placed on carbon, nitrogen and oxygen atoms and diffuse functions used for all atoms except for hydrogen. The geometry of the models was optimized by an analytical gradient method until the energy had converged to be better than $5 \cdot 10^{-5}$

Hartree/Bohr. The interaction energy of a Pt-group metal atom with an N-doped graphene fragment was calculated as: $E^{int} = E^{tot}(fragment) + E^{tot}(M) - E^{tot}(model)$, where $E^{tot}(fragment)$, $E^{tot}(M)$ and $E^{tot}(model)$ are the total energy of the isolated initial N-doped graphene fragment, of the single metal atom, and of the model, respectively. The interaction energy of formic acid (FA) in those models was calculated as: $E^{int} = E^{tot}(M\text{-}fragment) + E^{tot}(FA) - E^{tot}(model)$, where $E^{tot}(M\text{-}fragment)$, $E^{tot}(FA)$ and $E^{tot}(model)$ are the total energies of the isolated N-doped graphene fragment with anchored metal atom, free formic acid molecule and the model, respectively.

3. RESULTS AND DISCUSSION

Characterization of the catalysts and supports. The used carbon nanofibers possessed a herringbone-type and platelet structures (Figure S2, Supporting Information), irrespective of whether nitrogen was incorporated or not.[31, 36] These structures imply the presence of significant content of open edge sites (plane ends). There is a known problem of revealing the open edge sites of graphene layers as they can be covered by amorphous carbon formed as a result of interaction of the carbon containing samples with electron beam of a microscope. Additionally, the ends of the neighboring planes may close up under electron irradiation. Figure 1 shows a representative TEM image for one of the catalysts. It is seen that the diameter of the nanofiber corresponds to 20-30 nm. The planes of the nanofibers presented in Figure 1 end, since, when going through focus, the end remains. These open edge sites can be the places of location for metal species.

The high content of nitrogen in the N-doped samples (7 wt.%) allowed detailed characterization of nitrogen species by XPS. The XPS spectrum of the 1 wt.% Pd/N-CNFs catalyst in the N 1s region (Figure S3, Supporting Information) indicated the presence of pyridinic nitrogen species (398.8 eV), oxygen containing nitrogen species (404.6 eV), and pyrrolic/graphitic nitrogen species (unseparated line at 401.0 eV), the concentrations of pyridinic and pyrrolic/graphitic nitrogen being approximately the same.

We synthesized the catalysts by a method that affords highest metal dispersion, and a study with HAADF/STEM revealed the presence of nanoparticles with a mean size of 1.0 nm for Pt, 1.5 nm for Ru, and 2.3 nm for Pd in the supported samples with metal loading of 1 wt.%. The size distributions were quite narrow, with a standard deviation of 0.2-0.5 nm (Figure S4-S6, Supporting Information). It is important that nitrogen doping did not affect the mean particle size, if the same metal was considered (Table S1, Supporting Information). This allowed investigating the effect of nitrogen introduction into the support whilst neglecting the particle-size effect.

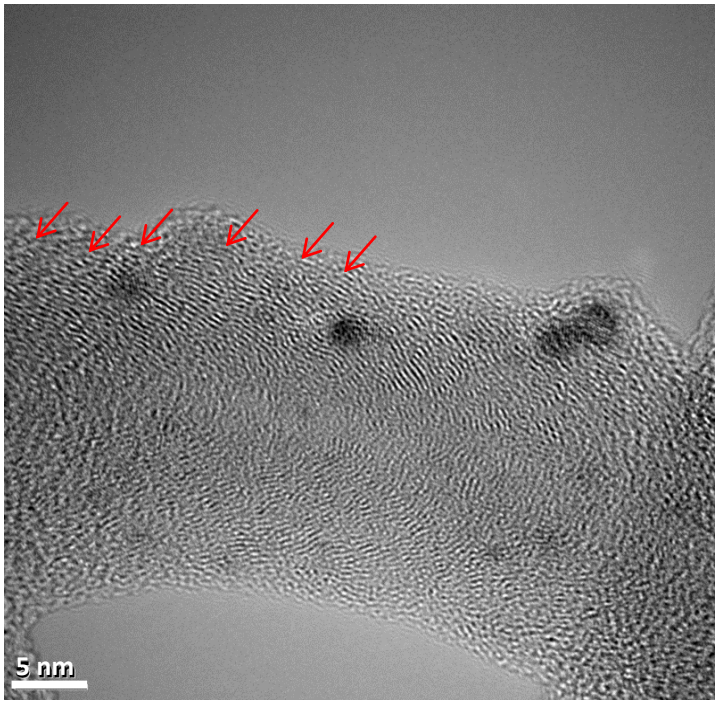

Figure 1. TEM image (JEM-2100F) of the 1 wt.% Pt/N-CNFs catalyst after testing of the sample in decomposition of formic acid. Arrows point to inclined, ending lattice planes.

In the case of spherical nanoparticles, the metal-particle sizes determined from JEM-2100F images correspond to metal dispersion (the fraction of metal atoms exposed to the surface, $D_{TEM} = M_{surface}/M_{total}$, calculated as indicated in Supporting Information) near 100, 90, and 50% for the Pt, Ru, and Pd catalysts, respectively. It implies that almost all metal atoms in Pt and Ru catalysts should be accessible to the reactants in a catalytic reaction, whereas half of the Pd atoms are present

in the bulk of nanoparticles. Since sub-nanometer sized metal species are invisible using a conventional (uncorrected) electron microscope, we have used CO chemisorption as a method that allows direct determination of the content of surface metal sites in the catalysts. CO is known to adsorb very strongly on Pt-group metals, being capable of replacing hydrogen from the metal surface even under H_2 pressure.[40,41] Earlier, we have applied this technique to a wide number of Pt catalysts, which were prepared on activated carbons and carbon blacks through hydrolytic (as in the present work) and reductive depositions, and obtained a good correspondence between the D_{CO} equal to the CO/Metal mole ratio and D_{TEM} values for these samples as well as a good correlation between the determined metal dispersions (D_{CO}) and catalytic properties of the samples both for structure-insensitive and structure-sensitive reactions.[42]

Figure 2a shows results of CO chemisorption measurements for the catalysts based on CNFs and N-CNFs supports. Contrary to the expectations from the data obtained with the JEM-2100F microscope, the Pt, Ru, and Pd samples on the N-free CNFs do not show a significant difference in CO/Metal ratios, and only for the Pd/CNFs catalyst did the D_{CO} value approach that (50%) expected from STEM measurements. This implies that many of the Pt and Ru atoms in the samples do not chemisorb CO, at least under the conditions used for the chemisorption measurements. Moreover, it is seen in Figure 2a that the nitrogen doping further decreases the amount of chemisorbed CO, in spite of the same metal particle size in the CNFs and N-CNFs-based samples (according to the measurements by JEM-2100F). Interestingly, the effect of nitrogen doping is most noticeable for Pt samples; the CO/Pt ratio for the 1 wt.% Pt/N-CNFs catalyst drops by a factor of 3.5 and the 0.3 wt.% Pt/N-CNFs sample does not adsorb CO at all.

The CNFs and N-CNFs used were exceptionally mesoporous. Hence, the content of micropores in the catalysts was small and the blockage of metal particles in the micropores as a possible reason for the decreased adsorption capacity can be ruled out. The presence (whatever the reasons) and strong effect of external contaminations is also unlikely, because the catalysts with the

decreased CO/Metal ratio demonstrated the highest catalytic activity, as will be shown below. It might be argued that the catalytic testing was performed at elevated temperature but the chemisorption measurements at ambient conditions. All our catalysts were reduced at a high temperature before their using, both for catalysis and for characterization. Before CO-chemisorption measurements, the samples were only re-reduced under milder conditions. As checked with separate samples, rising the temperature during re-reduction to 423-473 K or heating in helium at elevated temperature (523 K) prior to CO chemisorption responded negatively rather than positively on the CO/Metal values. Further evidence for the reduced ability of the N-CNF-supported samples to chemisorb CO comes from our earlier data showing an increased resistance of the Pt/N-CNFs catalysts to CO inhibition under the conditions of the formic acid decomposition; after introduction of CO to the feed, the activity of the Pt/CNFs sample decreased 10 times, whereas in the case of Pt/N-CNFs catalyst the decrease was only by a factor of 2.5.[31]

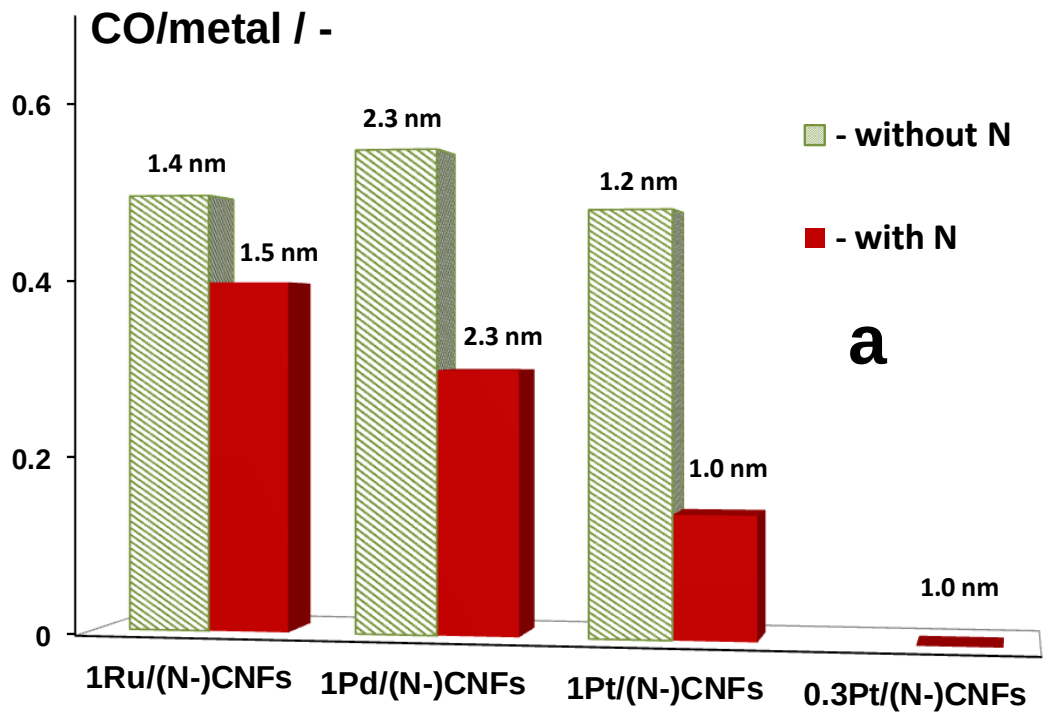

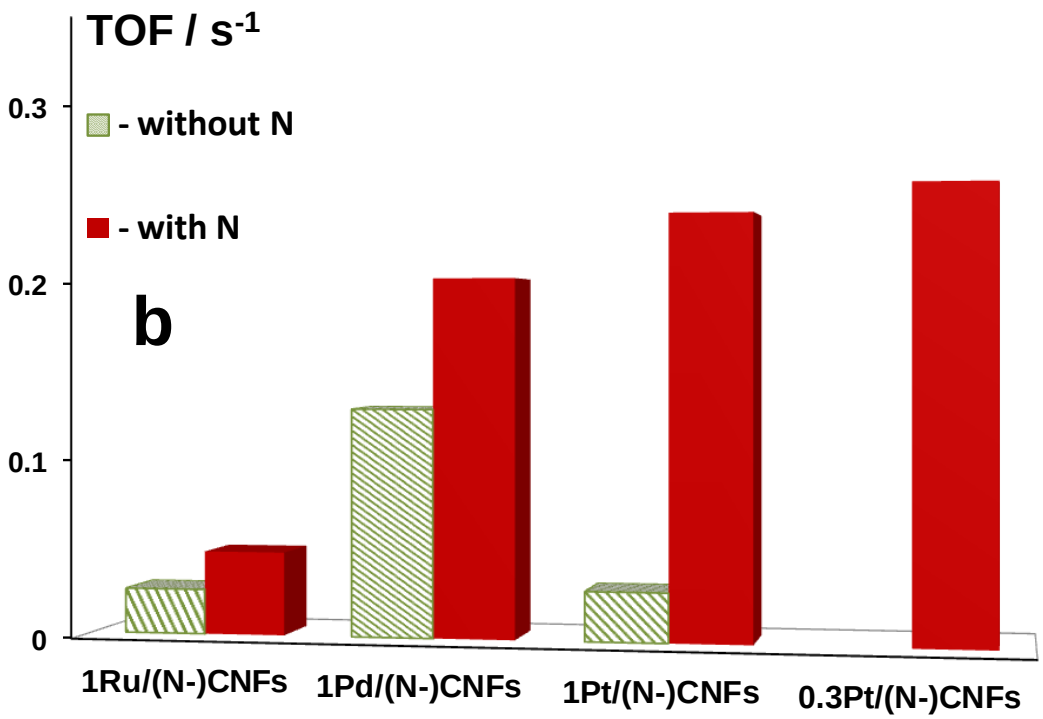

Figure 2. Effect of the metal nature and nitrogen doping on the (a) CO/Metal mole ratio and (b) TOF values in the formic acid decomposition at 398 K. In panel (a), the data for the mean size of nanoparticles visible by the JEM-2100F microscope are provided for comparison.

All that leads to the suggestion that the strong changes in the CO chemisorptions properties are a consequence of the strong interaction of the metal species with the support. It is confirmed by the observation of many single metal atoms in the samples, especially on the N-doped CNFs (to be considered further in more detail). It is reasonable to suggest that the strong interaction with the support drastically changes the electronic state of the metal atoms. Indeed, the XPS data for the samples (see later) clearly show that the state of metal atoms becomes similar to the state of metal ions in metal complexes in spite of the reduction performed *ex situ*. This will inevitably weaken the back-donation of metal d-electrons to π^* antibonding orbital of CO, which is known to contribute substantially to the strength of the CO-Metal bond. For instance, CO adsorbs with smaller adsorption energy on a positively charged Pt_4 cluster, as compared to a neutral or negatively

charged clusters.[43] There are enough examples in the literature that the irreversible adsorption of CO is weakened and even can become undetectable, if the metal species are in an ionic/electron-deficient state.[14,15,19,43] Moreover, Vile et al.[19] did not detect any adsorption of CO on single ionic Pd atoms supported on carbon nitride, while these atoms were very active in some hydrogenation reactions.

The smaller effect of nitrogen doping on the CO/Metal ratios for the Ru and Pd catalysts in Figure 2a indicates a smaller content of ionic species in these samples. In its turn, the smaller effect of the support on the CO-adsorption ability of the 1 wt.% Pt/N-CNFs catalyst in comparison to that for the 0.3 wt.% Pt/N-CNFs catalyst (Figure 2a) indicates a limit in the number of surface support sites capable of strongly interacting with the metal. From the pronounced effect of the nature of the support (CNFs vs N-CNFs in Figure 2a) it follows that such sites are more abundant on the surface of N-containing CNFs. This could reflect either simple increase of the number of the sites or the appearance of new specific sites when the support is prepared in the presence of nitrogen donor. The latter is supported by the study performed by Arrigo et al.[14] and our recent electron spectroscopy study of the interaction of Pd with another type of N-doped carbon.[34] We consider the possible structures with nitrogen and metal atoms in the final parts this paper.

Catalytic activity. Figure 2b shows specific reaction rates determined for the formic acid decomposition on different catalysts. Here, the rates are given as turnover frequencies (TOF) and are related to the total number of metal atoms in a catalyst. The trend of the catalyst's activity remained essentially the same if comparison was made with the temperature, at which the conversion of formic acid reached 50% (Table S1, Supporting Information). We have shown earlier[31,32] that the CNFs and N-CNFs supports by themselves are not active in the reaction in the given temperature range. The catalytic activity of metal-containing samples is therefore a consequence of the presence of metal nanoparticles and/or atomic metal species.

Comparing the properties of the N-free catalysts in Figure 2b, one can see that the Pd catalyst demonstrates the highest activity in comparison to Pt and Ru catalysts. This is consistent with earlier observations by Tedsree et al.[44] for unsupported colloids of the same metals in the liquid-phase decomposition of formic acid. Those authors explained the difference in catalytic activity based on the d-band theory and strength of the formate species interaction with metal surfaces. The results for the Pt/CNFs and Pd/CNFs catalysts presented in Figure 2b also agree with our data for unsupported Pd and Pt powders with mean sizes of the particles of 25 and 9.3 nm, respectively. The TOF values for the unsupported Pd and Pt powders under identical conditions are equal to 0.133 and 0.021 s^{-1}, respectively (per surface metal atom in the given case), and these were similar to the TOF values for the supported N-free Pd and Pt catalysts (Figure 2b).

The CO chemisorption data for all catalysts indicate that the content of the sites chemisorbing CO is higher in the samples without nitrogen (Figure 2a). In accordance, the ethylene hydrogenation reaction over the 1 wt.% Pt/CNFs and 1 wt.% Pt/N-CNFs catalysts showed a similar trend.[31] Thus, the N-free catalyst demonstrated complete (100%) conversion of ethylene at 318 K while the N-doped catalyst showed the conversion of only 24%. As CO probes the metal sites on the surface of nanoparticles, the same sites are needed for the ethylene hydrogenation reaction.

In contrast, the formic acid decomposition reaction is strongly promoted by the presence of nitrogen in the support (Figure 2b, Table S1, Supporting Information). The difference in the TOFs reached an order of magnitude for the Pt catalysts providing the highest activity for the Pt containing N-doped catalyst among the studied catalysts. However, the TOF for the Pd catalyst supported on N-doped CNFs was not much lower than that for the Pt catalyst on the same support and 50% conversion was reached even at a lower temperature (Table S1, Supporting Information). The difference between the N-doped and N-free samples was smaller for the Pd and Ru catalysts (<2 times) in comparison to the Pt catalysts in accordance with a smaller difference in the CO/Metal ratios for these samples (Figure 2a).

It is very important and could be clearly seen in Figure 2b that the catalytic activity in the formic acid decomposition behaves in an opposite way in comparison to the CO/Metal ratios (Figure 2a). The catalysts with the lowest CO/Metal ratios demonstrate the highest activity (TOF). Thus, the 0.3 wt.% Pt/N-CNFs sample does not adsorb CO at all, but shows the highest TOF value. Evidently, this indicates that the sites mainly decomposing formic acid are different from those surface metal sites, which chemisorb CO irreversibly and perform the ethylene hydrogenation reaction. Hence, the increase of the activity of the catalysts with N-doping in the formic acid decomposition can be assigned to electron-deficient/ionic metal sites.

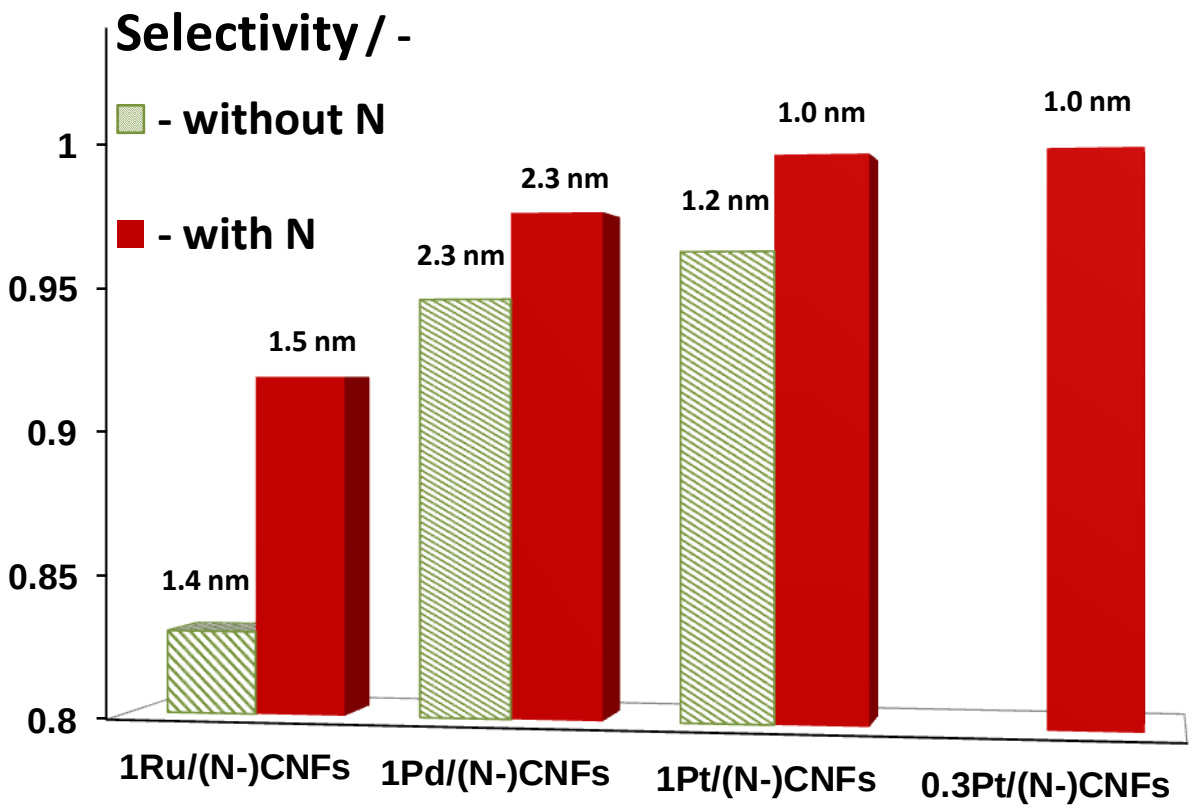

Figure 3. Effect of the metal nature and nitrogen doping on the selectivity for hydrogen production (at 50% conversion of formic acid). The TEM data for the mean size of metal nanoparticles visible by the JEM-2100F microscope are also provided.

It could be seen from Figure 3 that the trend of the hydrogen selectivity for the supported catalysts follows the order Pt (96-99.6%)>Pd (94-98%)>Ru (83-92%). For the Pt/N-CNFs catalysts, the selectivity reaches 99.6% being close to our detection limit of CO. It is important that the selectivity is always higher for the N-doped catalysts. The increase of the selectivity with N-doping indicates that the presence of ionic metal sites stabilized by nitrogen species leads to more selective catalyst. For the unsupported Pt and Pd powders, the selectivities were about 99% at 50% conversion. These values were lower than those for the Pt catalysts supported on N-doped carbon, but higher than those for other supported catalysts (Figure 3) indicating that the carbon supports and/or metal dispersion can affect the selectivity.

Single atoms of Pt and their stability. In an attempt to observe the single metal atoms, which are probably in the ionic state, we have carried out STEM imaging in the aberration-corrected Nion UltraSTEM 100 microscope. The bright field (left) and HAADF (right) STEM images of the 1 wt.% Pt/N-CNFs sample are presented in Figure 4. Note that the images show the sample after the reduction and catalytic testing at rather high temperatures (up to 573 K). It is near-impossible to reliably reveal the presence of Pt in bright field STEM (or TEM) images. In contrast, the HAADF images show the presence of Pt clusters of several tens of atoms, from mono-layer up to few (typically 2-3) layers thick, as well as single atoms of significantly higher brightness than the carbon or nitrogen of the support, because of their strong Z-contrast. To confirm that the single atoms are also Pt, intensity profiles were obtained from HAADF images along lines crossing individual atoms and near-by cluster atoms in locations, where the carbon support shows equal contrast and, hence, is of equal thickness. The pure (background subtracted) signal of the brightest single atoms is typically equal to or 2-3 times weaker than that of brightest atoms on the top of clusters, consistent with the conclusion that they are Pt and not Ni or Cu, the atoms of which might give about 5.5 times lower intensity in comparison to the Pt atoms. Although this consideration is imposed with some uncertainty, it undeniably supports the conclusion that the bright single atoms, seen in Figure 4 to a large fraction, are Pt atoms.

Moreover, a comparison of the bright field and HAADF images suggests that a considerable fraction of the Pt atoms is located on edge sites at the end of graphene sheets. Thus, the arrows in Figure 4 indicate some Pt atoms in the HAADF image and equivalent places in the bright field

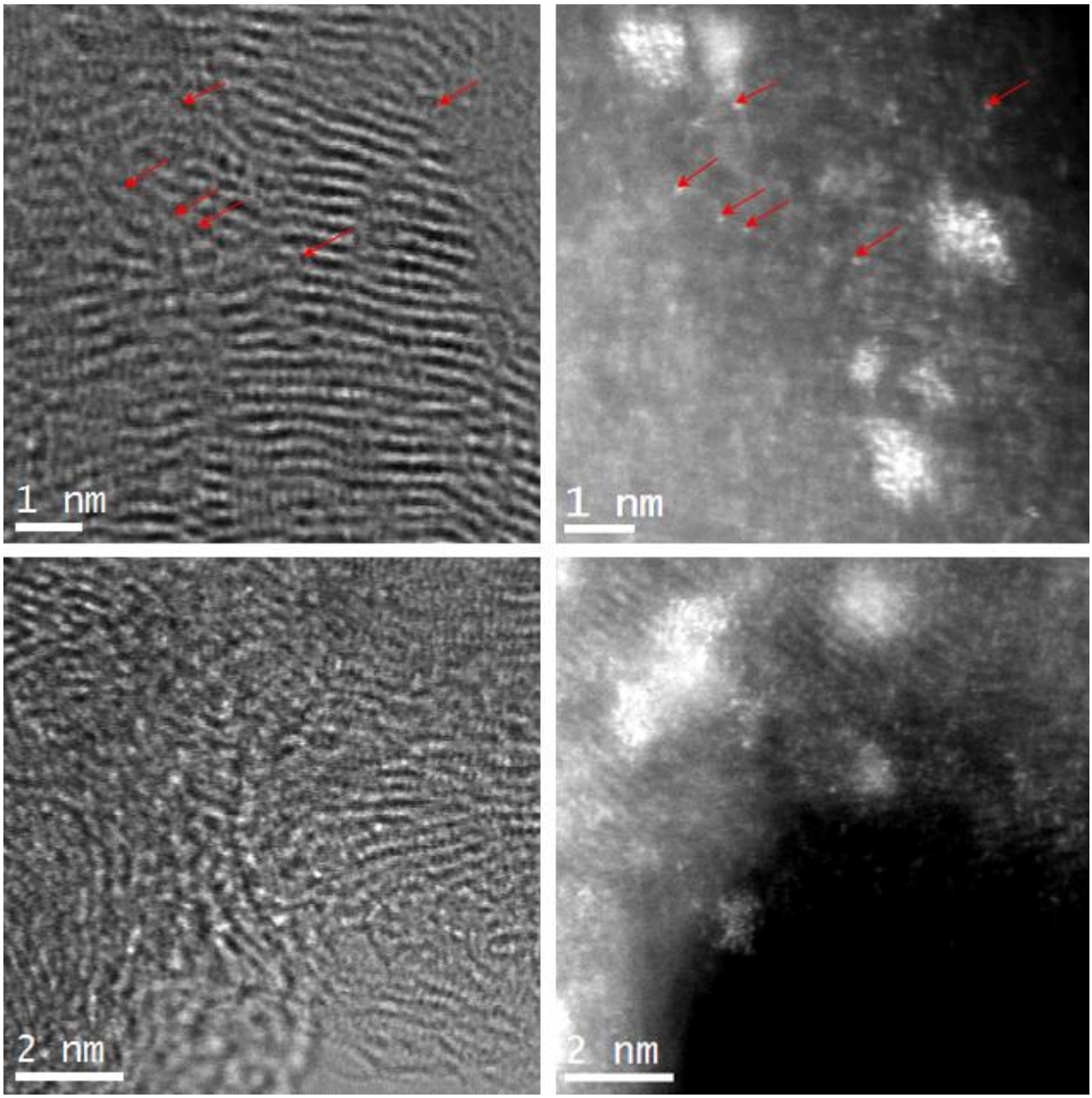

Figure 4. Bright field (left) and HAADF (right) STEM images (obtained in the Nion UltraSTEM 100) of the 1 wt.% Pt/N-CNFs catalyst after the decomposition of formic acid.

image. The atoms seem to sit in places where the sharpness of the lattice fringes is about to stop, i.e., where they go out of focus, meaning a stop of the progression of that lattice plane at that focus/height, so effectively meaning that there is an edge of that plane of some sort.

Hence, while it is difficult to determine quantitatively the exact nature of atomic species from the HAADF images alone, as this would require a precise knowledge of the support thickness, the intensity of these single atoms is qualitatively consistent with noble metals such as Pt. The CO chemisorption data for this sample (Figure 2a) indicate that more than 86% Pt is in this state. This is in line with the possible explanation of the effect of nitrogen incorporated into carbon supports, providing a strong interaction with ionic Pt-group metal atoms and preventing their sintering. HAADF/STEM observations of denoted sample areas and sequences of images (not shown here) taken over a time span of up to several minutes demonstrated no significant changes. A long term experiment performed for more than 40 h on stream with the same sample (1 wt.% Pt/N-CNFs)

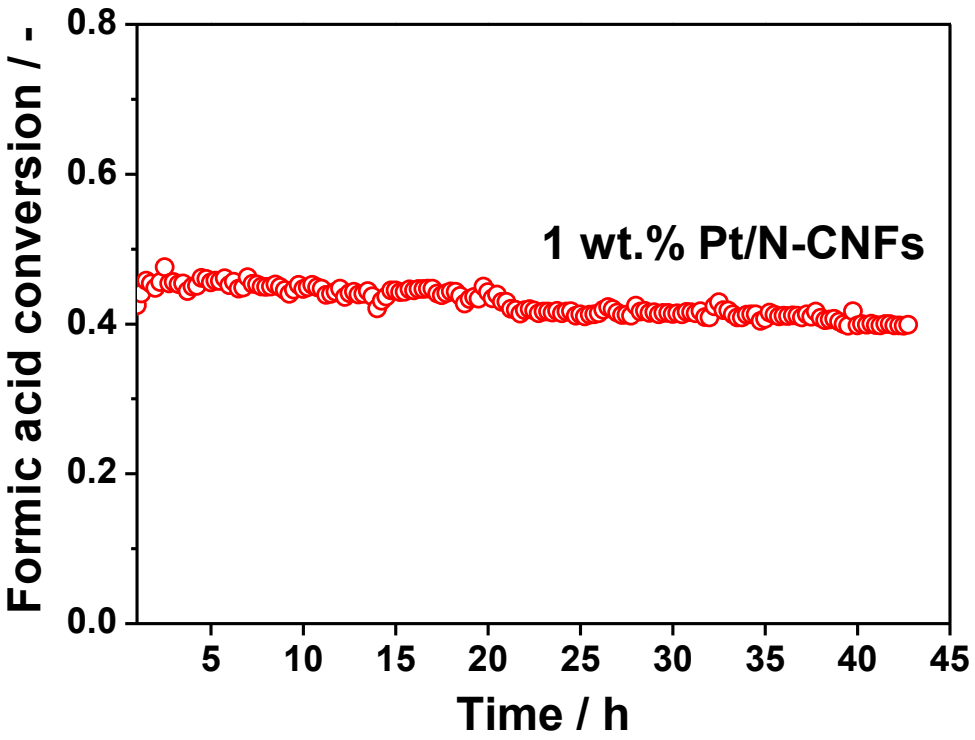

Figure 5. Long-term testing the 1 wt.% Pt/N-CNFs catalyst under the conditions of the formic acid decomposition at 448 K.

shown in Figure 5 indicates the very high stability of the active Pt sites under the conditions of formic acid decomposition.

XPS was used to determine the electronic state of metal in the samples reduced *ex situ* preventing their oxidation by air before the measurements. The studies of the 1 wt.% Pd/CNFs and especially 1 wt.% Pd/N-CNFs catalyst (Figure S7, Supporting Information) showed a considerable difference in comparison to the unsupported Pd powder after the same *ex situ* reduction.[34] The unsupported Pd powder demonstrated the presence of only metallic Pd, while the supported catalysts showed the presence of two forms of Pd: a highly dispersed metallic Pd (Pd^0, 335.7 eV)[14] and an ionic Pd (Pd^{2+},[14] 337.6 eV). The content of the ionic species was significant for both samples, but it was much higher for the N-doped sample than that for the N-free one. The presence of ionic Pd is assigned to stabilization of these species by nitrogen or oxygen species of the support. We showed recently for a Pd sample on another type of N-doped carbon using high-resolution photoelectron spectroscopy with synchrotron radiation that these unreducible Pd^{2+} species are attached to pyridinic nitrogen species incorporated on the carbon support and, very probably, are the active sites for the formic acid decomposition.[34]

Earlier, we have also studied electronic properties of the same Pt catalysts by XPS.[31] The Pt $4f_{7/2}$ binding energy for the *ex situ* reduced 1 wt.% Pt/N-CNFs catalyst was about 72.1 eV (Figure S8, Supporting Information), which is 1.0 eV higher than that for the unsupported Pt powder (71.1 eV). The Pt 4f binding energy for the N-doped catalysts significantly shifted by about 0.6 eV to higher values in comparison to the N-free sample[31] in spite of the similar mean Pt particle size for these samples determined by measurements in the JEM-2100F (Table S1, Supporting Information). The high range of binding energies indicated the presence of ionic Pt species with a few Pt atoms or even single Pt atoms[11] in the N-doped samples. Pt^{2+} ions in compounds such as $Pt(OH)_2$, PtO or PtS_2 provide binding energies in the same range (72-73 eV) pointing to the fact that the Pt species in the Pt/N-CNFs samples may correspond to the Pt^{2+} state also.

For the *ex situ* reduced Ru N-doped sample the Ru $3d_{5/2}$ binding energy (280.3 eV, Figure S8, Supporting Information) was also higher than that of the bulk Ru metal,[32] but the shift was not as strong as in the case of the Pt and Pd samples. It corresponded to 0.3 eV suggesting the presence of electron-deficient Ru species. Hence, the XPS data for the studied samples are in accordance with the CO chemisorption data indicating the presence of a significant content of ionic metal species in the N-doped samples.

In summary, among all studied samples, the 0.3 wt.% Pt/N-CNFs catalyst is a unique single-atom catalyst providing the highest activity (TOF) in the formic acid decomposition. The absence of the irreversible CO chemisorption on this sample (Figure 2a) and XPS data for the electronic state of Pt[31] point out that Pt is present mainly in the form of ionic species and that nanoparticles with a mean size of about 1.0 nm observed by conventional TEM (Figure S1, Supporting Information) are only representative of a small fraction of the total content of Pt, most of which is atomically dispersed and evidence for which is given in the HAADF image (Figure 4). However, the difference between the 0.3 and 1 wt.% Pt/N-CNFs samples is not significant. The latter sample contains only 14% of Pt atoms able to adsorb CO (Figure 2a). The increased content of nanoparticles for this sample is confirmed by HAADF/STEM images (Figure S1, Supporting Information) and particle size distributions (Figure S4, Supporting Information). The activity of the single Pt atom of this catalyst is more than one order of magnitude higher than that of the metal Pt atom in the unsupported Pt powder. This can be explained by the formation of single Pt atoms stabilized by nitrogen sites of the support. The selectivity is close to 100% (Figure 3) implying the CO-free production of hydrogen.

Location of single atoms of Pt-group metals. To define the location of single atoms of Pt-group metals and confirm their participation in the decomposition of formic acid, DFT calculations of model systems have been performed. For this, we constructed several models of graphene fragments containing nitrogen atoms bonded with three (graphitic nitrogen, N_{gr}) or two (pyridinic

nitrogen, N_{py}) carbon neighbors. These nitrogen species were chosen based on the XPS N 1s spectrum of N-CNFs, which showed two main peaks at 398.8 and 401.0 eV corresponding to pyridinic and graphitic nitrogen species (Figure S3, Supporting Information). The choice of these models is supported by the structure of the used carbon nanofibers as containing open edges (Figure 1, Figure 4, and Figure S2, Supporting Information). The observation of Pt atoms on the edge sites (Figure 4) is also in favor of the used models.

As an active site for the attachment of a Pt-group metal atom, we considered a single N_{gr} atom substituting a central carbon atom in a graphene fragment, one and two N_{py} atoms located on a vacancy and a pair of N_{py} atoms on the armchair or zigzag graphene edge (Figure S5, Supporting Information). The energies of interaction of single Pt, Pd and Ru atoms with these nitrogen species are compared in Table S2 (Supporting Information). All Pt-group metal atoms interact strongly with N_{py} sites. They stick to a two-atomic vacancy (divacancy) by forming four bonds with the boundary nitrogen and carbon atoms (Figure S9a, Supporting Information). The interaction of the Pt atom with a monovacancy containing one N_{py} atom is so energetically favorable that the C-C bond in the pentagon ring is broken and these atoms are linked to the metal atom (Figure S9b, Supporting Information). The metal atom binds to two N_{py} atoms, when this pair is located on the armchair edge of graphene (Figure S9c, Supporting Information), and to a single N_{py} atom, when a pair of N atoms is on the zigzag edge (Figure S9d, Supporting Information). The interaction with the edge N_{py} sites is significantly weaker than that with the vacancy N_{py} atoms (Table S2, Supporting Information). The smallest values for the interaction energy are obtained for the graphene fragment containing the N_{gr} site. The Pt and Pd atoms do not attach to this site, but are located over the center of the adjacent C–C bond (Figure S9e, Supporting Information). This is in line with the DFT calculations performed earlier with carbon nanotube fragments.[45] In contrast, the Ru atom interacts directly with the N_{gr} nitrogen atom and additionally with two carbon atoms neighboring this atom (Figure S9f, Supporting Information). Independent of the type of N site, the trend for the strength of interaction of metal atoms with a particular site follows Ru>Pt>Pd. By comparing this trend with

the catalytic activity of the corresponding metals supported on the N-CNFs (Figure 2b), we conclude that for the effective hydrogen production from formic acid decomposition the interaction of the metal atom with the support should not be too strong as in the case of Ru. The interaction of the Pd atoms with the N-sites is too weak in comparison to the Pt atoms and this may lead to sintering of metal and deactivation of the catalyst.

The charges on the Pt atoms interacting with N-carbon support were calculated using natural bond orbital (NBO) analysis (Table 1). It is seen that the Pt atom is electron-deficient, when it is attached to N_{py} sites, except for the case when it is nearly neutral being attached to a pair of N_{py} atoms at the zigzag edge. In contrast, the attachment at a location close to the N_{gr} atoms leads to some shift of electron density from the graphene fragment to Pt. It is consistent neither with the XPS data, which indicate a positive charge on metal atoms, nor with the CO chemisorption data, which reflect weakening of CO-M bond (M-metal atom) expected for the positively charged metal. This may indicate that the content of the M-(N_{gr}) and M-(2 N_{py}, zigzag) sites in the samples is low.

Table 1 Natural bond orbital (NBO) charge (*e*) on the Pt atom supported in different positions of the N-doped graphene and interaction energy (eV) of the formic acid molecule with the Pt atom, calculated at the PBE/LACVP level.

N site	2 N_{py} on divacancy	1 N_{py} on monovacancy	N_{gr} central	2 N_{py} armchair	2 N_{py} zigzag	1 N_{py} zigzag
NBO charge	+0.61	+0.51	-0.11	+0.24	-0.06	+0.17
Interaction energy	0.47	0.10	0.67	3.36	2.57	0.41

Formic acid interaction with single atoms of Pt-group metals. Furthermore, we have studied the interaction of the formic acid molecule with a Pt atom in all above-mentioned configurations of N-doped graphene fragments (Table S2, Figure S9, Supporting Information). The molecule was adsorbed on the Pt atom attached to the N_{py} atoms in vacancies (Figure 6a and Figure S10a) or near the N_{gr} atom (Figure 6b). The hydrogen atom from the –OH group of the formic acid molecule points to the metal atom. In the case when the Pt atom is attached to a pair of N_{py} atoms located on the armchair or zigzag graphene edge, the formic acid molecule dissociates with the formation of an adsorbed hydrogen atom and a carboxyl fragment (Figure 6c and Figure 6d). Interestingly the Pt atom is linked to both N_{py} atoms in the zigzag configuration after the formic acid interaction (Figure 6d), while it is linked only to one N_{py} atom in the initial state (Figure S9d, Supporting Information). It is important that the formic acid molecule is not able to dissociate on the Pt atom attached to the zigzag graphene edge with a single N_{py} atom (Figure S10b, Supporting Information). The energies of the interaction of formic acid with supported Pt atoms are collected in Table 1. The strongest interaction of the molecule resulting in dissociation is provided only by the Pt atoms bonded with a pair of the N_{py} sites on a graphene edge. Other sites could be considered as inactive.

Finally, we compared the interaction of formic acid with different Pt-group metal atoms attached to a pair of N_{py} atoms on the armchair edge. The interaction of the molecule with the Pd atom produces a configuration (Figure S6c, Supporting Information) similar to that for the Pt atom (Figure 6c). A significant feature of the decomposition on these atoms is that the formed adsorbed hydrogen atom and hydrogen of the carboxyl fragment are directed towards each other. The distance between them is relatively small (1.89 and 1.97 Å). This could provide an easy formation of hydrogen and CO_2 molecules. However, despite of the fact that the formic acid molecule also dissociates on the Ru atom (Figure 6e); the distance between the hydrogen atoms in that structure is sufficiently large (3.38 Å). The Ru atom located near the central single N_{gr} atom also provides the dissociation of the formic acid molecule (Figure 6f), but the distance between the hydrogen atoms is also large (2.76 Å). The difference in the configurations of formic acid with the Ru atom in

comparison to the Pt and Pd atoms could complicate the formation of the necessary H_2 product. In accordance, the activity of the formic acid decomposition on the Ru catalysts was the lowest (Figure 2b) and the experimental apparent activation energy of the formic acid dehydrogenation for the N-doped Ru catalyst was equal to 57 kJ mol^{-1},[32] which was 6 kJ mol^{-1} higher than that for the N-doped Pd catalyst.

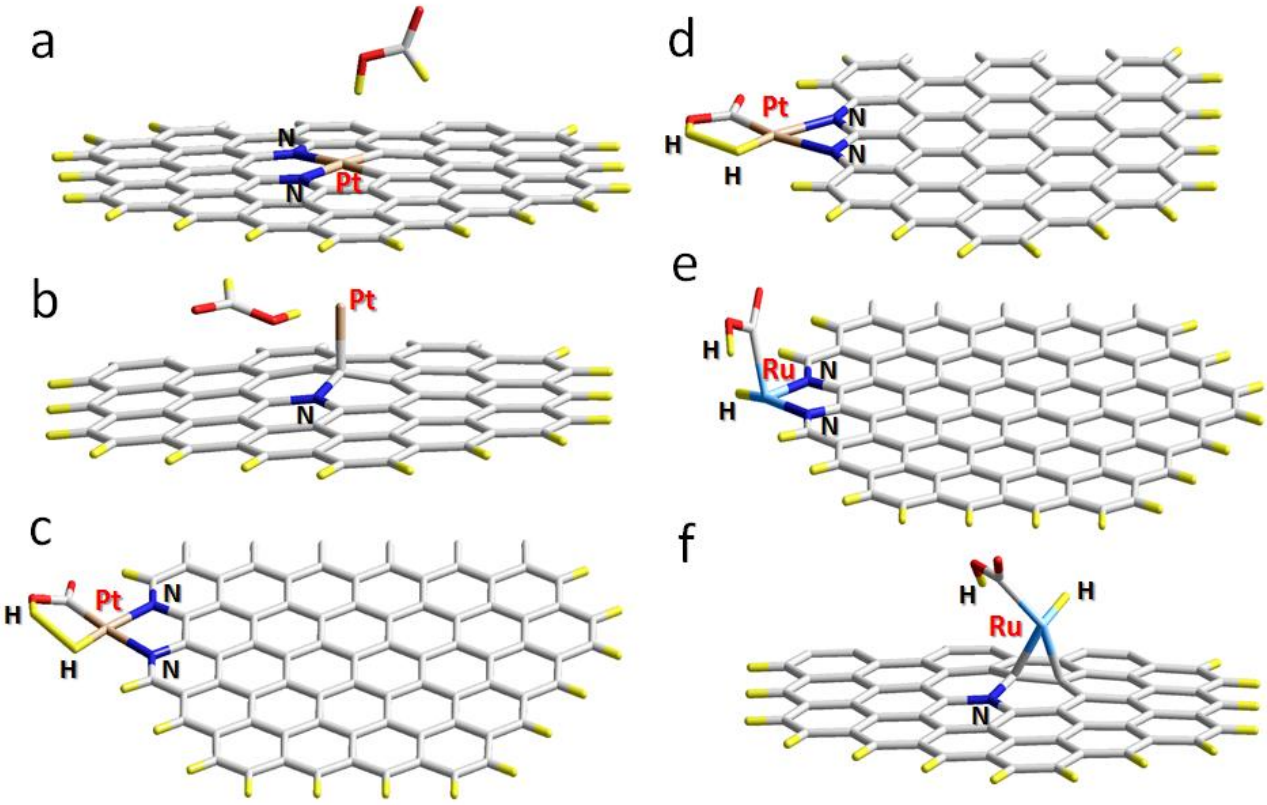

Figure 6. Geometries of models with the formic acid molecule above Pt and Ru atoms located in different positions in nitrogen-containing graphene fragments optimized at PBE/LACVP*+ level. Interaction of the formic acid molecule with (a) a Pt atom attached to the divacancy with two pyridinic N atoms, (b) a Pt atom attached near the graphitic type N atom, (c) a Pt atom attached to two pyridinic N atoms on the armchair edge, (d) a Pt atom attached to two pyridinic N atoms on the zigzag edge, (e) a Ru atom attached to two pyridinic N atoms on the armchair edge, and (f) a Ru atom attached near the graphitic type N atom. Blue colour indicates N, red – O, yellow – H.

Outlook. The single Pt or Pd atoms attached to a pair of nitrogen atoms on the edge in the armchair configuration manifest themselves as the most promising candidates for advanced catalysts with exceptional properties in the formic acid decomposition. Such active sites are similar in structure to Pt-group metal complexes with 2,2'-bipyridine or 1,10-phenanthroline, but the isolation of the active sites from each other provides stability under the conditions of catalytic reaction (Figure 5). The possibility of creating such active sites via proper doping of CNFs with nitrogen has made it possible to achieve nearly 100% selectivity to H_2 and to enhance activity by an order of magnitude (Figure 2b and Figure 3). It does not mean that our catalysts are composed exclusively from the sites shown in Figure 6c; there are usual metal clusters (Figure 4) and it can be low active or inactive single metal atoms with an enhanced stability (as shown in Figure 6a). As the fraction of the most active sites may be low, the high level of the total activity implies that some of the sites exceed in activity the heterogeneous metal catalysts by more than one order of magnitude. The data for homogeneous catalysts are in favor for this consideration, as the catalytic activity of some metal complexes with nitrogen containing chelating ligands, representing, in fact, single-site catalysts, is significantly higher than that of the heterogeneous catalysts.[1,2,46] Hence, there is enough room for further optimization of the catalysts by increasing the content of the most active supported single atoms. Yet, it will be a very challenging task demanding a delicate balance between the catalyst's activity and stability. Further insights into new applications could assist in the developing of these catalysts. At the moment, such catalysts seem promising at least for hydrogen production reactions via decomposition of different chemical compounds containing hydrogen (CH_3OH, HCHO, C_nH_{2n+2}, NH_3, etc.) at low temperatures.

4. CONCLUSIONS

The N-doped carbon-supported catalysts with single atoms of Pt-group metals have proven capable of providing a remarkably high rate of formic acid decomposition, along with excellent selectivity

to H_2 and CO_2 and the possibility of using low loadings of Pt-group metals. The catalyst support could be easily obtained by pyrolysis of hydrocarbons in the presence of N-donors, and the catalysts are easily prepared from conventional metal precursors through hydrolytic deposition on the support. The observations with aberration-corrected HAADF/STEM give direct evidence for the thermal stability of the resulting supported metal atoms, providing the opportunity of using the synthesized single-atom catalysts at temperatures up to 573 K. Contrarily to nanoparticles and nanoclusters, the anchored metal atoms show low activity in ethylene hydrogenation and do not chemisorb CO irreversibly at ambient temperature, thereby indicating a strongly electron-deficient or ionic state of the metal atoms, as in metal complexes. This is consistent with the XPS data and explains why these single metal atoms do not aggregate.

The DFT modeling revealed a strong stabilization of the individual metal atom by a pair of pyridine-type nitrogen atoms located at the open edge of the graphene sheet. The formation of such active sites enhances the reaction rate up to 10 times in comparison to the N-free catalysts, while improving the selectivity to H_2. This opens a possibility of obtaining hydrogen from renewable resources which would not require the cost-ineffective and time-consuming purification from CO admixtures. The N-doped carbon nanofibers used here could therefore be considered as a kind of efficient and stable macro-ligand, which possesses excellent chelate properties and allows the advantages of heterogeneous and homogeneous catalysts to be successfully combined. There are good reasons to believe that the findings could be extended to other kinds of single-atom catalysts and will be helpful in improving the energy-related and environmentally benign processes.

ASSOCIATED CONTENT

Supporting Information

The Supporting Information is available free of charge on the ACS Publications website at DOI:

Temperature of 50% conversion and mean particle size of the catalysts (Table S1), interaction energies of isolated noble metal atoms with different nitrogen defects (Table S2), HAADF/STEM images (Figure S1), N 1s and Pd 3d spectra (Figure S3 and S7), particle size distributions for the catalysts (Figures S4-S6), Pt 4f and Ru $3d_{5/2,}$ XPS spectra (Figure S8), models of attachment of Pt and Ru atoms (Figure S9) and geometries of models with formic acid molecule over Pt and Pd atoms (Figure S10).

AUTHOR INFORMATION

Corresponding Authors

*E-mail: dmitri.bulushev@catalysis.ru

Notes

The authors declare no competing financial interest.

ACKNOWLEDGMENTS

This publication has emanated from research conducted with the financial support of the Russian Science Foundation (Grant 16-13-00016). M.Z. acknowledges the support of the Earth and Natural Sciences (ENS) Doctoral Studies Programme, funded by the Higher Education Authority (HEA) through the Programme of Research at Third Level Institutions, Cycle 5 (PRTLI – 5), co-funded by the European Regional Development Fund (ERDF). The electron microscopy results presented here were obtained at microscopes of the University of Limerick (JEM-2100F) and the Daresbury Laboratories (SuperSTEM), the U.K. National Midrange Facility for Aberration-Corrected STEM, funded by the Engineering and Physical Sciences Research Council (EPSRC). The authors appreciate highly the assistance and support by Drs. S. Beloshapkin, A. Boronin, L. Jia, E. Gerasimov, Y. Guo, Z. Ismagilov, L. Kibis, J.J. Leahy, A. Okotrub, V. Parmon, J. Ross and O. Taran.

REFERENCES

(1) Grasemann, M.; Laurenczy, G. *Energy Environ. Sci.* **2012**, *5*, 8171-8181.

(2) Loges, B.; Boddien, A.; Gartner, F.; Junge, H.; Beller, M. *Top. Catal.* **2010**, *53*, 902-914.

(3) Enthaler, S.; von Langermann, J.; Schmidt, T. *Energy Environ. Sci.* **2010**, *3*, 1207-1217.

(4) Sponholz, P.; Mellmann, D.; Junge, H.; Beller, M. *ChemSusChem* **2013**, *6*, 1172-1176.

(5) Singh, A. K.; Singh, S.; Kumar, A. *Catal. Sci. Technol.* **2016**, *6*, 12-40

(6) Hayes, D. J.; Fitzpatrick, S.; Hayes, M. H. B.; Ross, J. R. H. In *Biorefineries-Industrial Processes and Products*; Kamm, B., Gruber, P. R., Kamm, M., Eds.; Wiley-VCH: Weinheim, 2006; Vol. 1, p 139-164.

(7) Li, J.; Ding, D. J.; Deng, L.; Guo, Q. X.; Fu, Y. *ChemSusChem* **2012**, *5*, 1313-1318.

(8) Bulushev, D. A.; Ross, J. R. H. *Catal. Today* **2011**, *163*, 42-46.

(9) Serrano-Ruiz, J. C.; Braden, D. J.; West, R. M.; Dumesic, J. A. *Appl. Catal., B* **2010**, *100*, 184-189.

(10) Thomas, J. M. *Design and Applications of Single-Site Heterogeneous Catalysts*; Imperial College Press: London, 2012, p 1-293.

(11) Bruix, A.; Lykhach, Y.; Matolinova, I.; Neitzel, A.; Skala, T.; Tsud, N.; Vorokhta, M.; Stetsovych, V.; Sevcikova, K.; Myslivecek, J.; Fiala, R.; Vaclavu, M.; Prince, K. C.; Bruyere, S.; Potin, V.; Illas, F.; Matolin, V.; Libuda, J.; Neyman, K. M. *Angew. Chem., Int. Ed.* **2014**, *53*, 10525-10530.

(12) Yang, X. F.; Wang, A. Q.; Qiao, B. T.; Li, J.; Liu, J. Y.; Zhang, T. *Acc. Chem. Res.* **2013**, *46*, 1740-1748.

(13) Kochubey, D. I.; Chesnokov, V. V.; Malykhin, S. E. *Carbon* **2012**, *50*, 2782-2787.

(14) Arrigo, R.; Schuster, M. E.; Xie, Z.; Yi, Y.; Wowsnick, G.; Sun, L. L.; Hermann, K. E.; Friedrich, M.; Kast, P.; Havecker, M.; Knop-Gericke, A.; Schlogl, R. *ACS Catal.* **2015**, *5*, 2740-2753.

(15) Peterson, E. J.; DeLaRiva, A. T.; Lin, S.; Johnson, R. S.; Guo, H.; Miller, J. T.; Kwak, J. H.; Peden, C. H. F.; Kiefer, B.; Allard, L. F.; Ribeiro, F. H.; Datye, A. K. *Nat. Commun.* **2014**, *5*, 4885.

(16) Yan, H.; Cheng, H.; Yi, H.; Lin, Y.; Yao, T.; Wang, C.; Li, J.; Wei, S.; Lu, J. *J. Am. Chem. Soc.* **2015**, *137*, 10484-10487.

(17) Moses-DeBusk, M.; Yoon, M.; Allard, L. F.; Mullins, D. R.; Wu, Z.; Yang, X.; Veith, G.; Stocks, G. M.; Narula, C. K. *J. Am. Chem. Soc.* **2013**, *135*, 12634-12645.

(18) Narula, C. K.; Allard, L. F.; Stocks, G. M.; Moses-DeBusk, M. *Sci. Rep.* **2014**, *4*, 7238.

(19) Vile, G.; Albani, D.; Nachtegaal, M.; Chen, Z.; Dontsova, D.; Antonietti, M.; Lopez, N.; Perez-Ramirez, J. *Angew. Chem., Int. Ed.* **2015**, *54*, 11265-11269.

(20) Zhang, X.; Shi, H.; Xu, B. Q. *Angew. Chem., Int. Ed.* **2005**, *44*, 7132-7135.

(21) Hackett, S. E. J.; Brydson, R. M.; Gass, M. H.; Harvey, I.; Newman, A. D.; Wilson, K.; Lee, A. F. *Angew. Chem., Int. Ed.* **2007**, *46*, 8593-8596.

(22) Sun, S. H.; Zhang, Z. J.; Gauquelin, N.; Chen, N.; Zhou, J.; Yang, S.; Chen, W.; Meng, X.; Geng, D.; Banis, M. N.; Li, R. Y.; Ye, S. Y.; Knights, S.; Botton, G. A.; Sham, T. K.; Sun, X. L. *Sci. Rep.* **2013**, *3*, 1775.

(23) Belyi, A. S.; Smolikov, M. D.; Kir'yanov, D. I.; Udras, I. E. *Russ. J. Gen. Chem.* **2007**, *77*, 2243-2254.

(24) Yi, N.; Saltsburg, H.; Flytzani-Stephanopoulos, M. *ChemSusChem* **2013**, *6*, 816-819.

(25) Flytzani-Stephanopoulos, M. *Acc. Chem. Res.* **2014**, *47*, 783-792.

(26) Ciftci, A.; Ligthart, D.; Pastorino, P.; Hensen, E. J. M. *Appl. Catal., B* **2013**, *130*, 325-335.

(27) Ojeda, M.; Iglesia, E. *Angew. Chem., Int. Ed.* **2009**, *48*, 4800-4803.

(28) Kwak, J. H.; Kovarik, L.; Szanyi, J. *ACS Catal.* **2013**, *3*, 2094-2100.

(29) Podyacheva, O. Y.; Ismagilov, Z. R. *Catal. Today* **2015**, *249*, 12-22.

(30) Wood, K. N.; O'Hayre, R.; Pylypenko, S. *Energy Environ. Sci.* **2014**, *7*, 1212-1249.

(31) Jia, L. J.; Bulushev, D. A.; Podyacheva, O. Y.; Boronin, A. I.; Kibis, L. S.; Gerasimov, E. Y.; Beloshapkin, S.; Seryak, I. A.; Ismagilov, Z. R.; Ross, J. R. H. *J. Catal.* **2013**, *307*, 94-102.

(32) Zacharska, M.; Podyacheva, O. Y.; Kibis, L. S.; Boronin, A. I.; Senkovskiy, B. V.; Gerasimov, E. Y.; Taran, O. P.; Ayusheev, A. B.; Parmon, V. N.; Leahy, J. J.; Bulushev, D. A. *ChemCatChem* **2015**, *7*, 2910-2917.

(33) Marco, Y.; Roldan, L.; Armenise, S.; Garcia-Bordeje, E. *ChemCatChem* **2013**, *5*, 3829-3834.

(34) Bulushev, D. A.; Zacharska, M.; Shlyakhova, E. V.; Chuvilin, A. L.; Guo, Y.; Beloshapkin, S.; Okotrub, A. V.; Bulusheva, L. G. *ACS Catal.* **2016**, *6*, 681-691.

(35) Shalagina, A. E.; Ismagilov, Z. R.; Podyacheva, O. Y.; Kvon, R. I.; Ushakov, V. A. *Carbon* **2007**, *45*, 1808-1820.

(36) Kaprielova, K. M.; Yakovina, O. A.; Ovchinnikov, I. I.; Koscheev, S. V.; Lisitsyn, A. S. *Appl. Catal., A* **2012**, *449*, 203-214.

(37) Krivanek, O. L.; Corbin, G. J.; Dellby, N.; Elston, B. F.; Keyse, R. J.; Murfitt, M. F.; Own, C. S.; Szilagyi, Z. S.; Woodruff, J. W. *Ultramicroscopy* **2008**, *108*, 179-195.

(38) Jia, L.; Bulushev, D. A.; Beloshapkin, S.; Ross, J. R. H. *Appl. Catal., B* **2014**, *160*, 35-43.

(39) Perdew, J. P.; Burke, K.; Ernzerhof, M. *Phys. Rev. Lett.* **1996**, *77*, 3865.

(40) Gurrath, M.; Kuretzky, T.; Boehm, H. P.; Okhlopkova, L. B.; Lisitsyn, A. S.; Likholobov, V. A. *Carbon* **2000**, *38*, 1241-1255.

(41) Okhlopkova, L. B.; Lisitsyn, A. S.; Likholobov, V. A.; Gurrath, M.; Boehm, H. P. *Appl. Catal. A* **2000**, *204*, 229-240.

(42) Kaprielova, K. M.; Ovchinnikov, I. I.; Yakovina, O. A.; Lisitsyn, A. S. *ChemCatChem* **2013**, *5*, 2015-2024.

(43) Tang, Y. N.; Yang, Z. X.; Dai, X. Q. *J. Nanoparticle Res.* **2012**, *14*, 844.

(44) Tedsree, K.; Li, T.; Jones, S.; Chan, C. W. A.; Yu, K. M. K.; Bagot, P. A. J.; Marquis, E. A.; Smith, G. D. W.; Tsang, S. C. E. *Nat. Nanotechnol.* **2011**, *6*, 302-307.

(45) Li, Y. H.; Hung, T. H.; Chen, C. W. *Carbon* **2009**, *47*, 850-855.

(46) Himeda, Y. *Green Chem.* **2009**, *11*, 2018-2022.
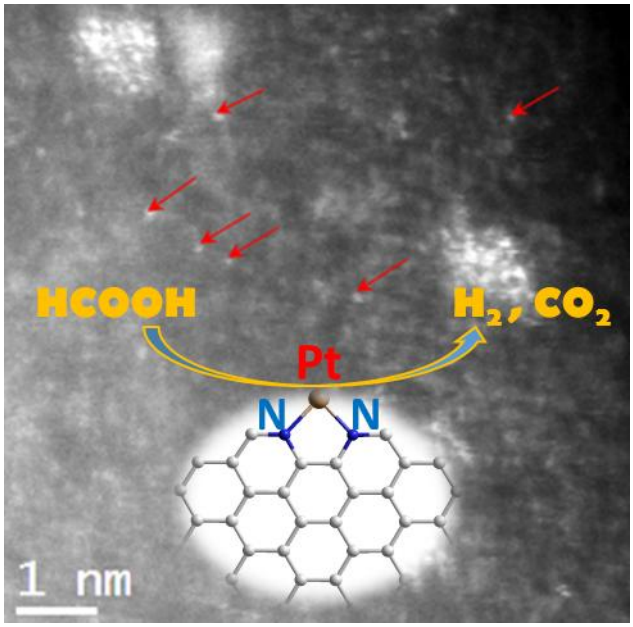
TOC Graphic